Design of a Broadband Circularly Polarized Antenna by Using Axial Ratio Contour

Lehu Wen, Steven Gao, *Fellow, IEEE,* Qi Luo, *Senior Member, IEEE,*
Wei Hu, *Member, IEEE,* and Benito Sanz-Izquierdo

***Abstract*—A novel method of using axial ratio (AR) contour to design a broadband circularly polarized (CP) antenna is presented in this letter. By resolving a radiated CP wave into two orthogonal far-field components, the resulted AR will be determined by the radiated power and phase differences between the two orthogonal components. Therefore, a series of AR contours can be obtained for different AR values of the radiated wave. In the AR contour, details of phase-advance, phase-lag, power-advance, and power-lag can be simultaneously observed along with the resulted AR. Based on these analyses, the AR contour is first utilized to directly design a broadband CP antenna instead of using the traditional AR versus frequency curve to achieve optimal AR bandwidth. Compared to the traditional AR curve, the method of using AR contour to design CP antenna is more effective and informative. The designed broadband CP antenna was also fabricated and measured for the final performance verification.**

***Index Terms*—Axial ratio, broad bandwidth, circularly polarized antenna.**

I. Introduction

CIRCULARLY polarized (CP) antennas can reduce the multi-path fading effect, increase the communication channel capacity, and have the advantage of orientation flexibility between the transmitting and receiving antennas [1]. Therefore, CP antennas have been widely applied in many wireless communication systems, such as satellite, radio frequency identification, navigation, radar, etc. With the fast development of these systems, increasingly wider impedance and axial ratio (AR) bandwidths are required for CP antennas.

To obtain broad impedance bandwidth for unidirectional CP radiation, crossed dipoles are commonly used in these antenna designs. By using the integrated phase delay lines [2]-[7] and the self-phased dipole arms [8]-[10], wideband CP dipole antennas are developed. With the help of arc-shaped phase delay line, rectangular strips [2] and L-shaped strips [3] are excited for CP radiation. To further improve the bandwidth for CP radiation, crossed loops [4], corner chamfered square patches [5], and slot etched polygonal patches [6] are utilized for parasitic radiation with the enhanced AR bandwidth. In addition, by using the internal phase difference between the small and large loops, a cavity-backed CP antenna with simple structure and enhanced gain is presented in [8]. With the help of the travelling current on the S-shaped dipole arm [10], AR bandwidth of 60% is achieved with the wide AR beamwidth. In addition, by using series-feed method [11]-[12] and quadrature feed networks [13]-[15], broadband antennas are achieved for the stable unidirectional CP radiation.

In these designs, single AR curve is normally used to directly characterize the required AR bandwidth. However, how to obtain and control the background information of the radiated waves to achieved broad AR bandwidth is always neglected. To analyze the background information of the resulted AR, the radiated orthogonal far-field components are researched for detailed illustration of the resulted AR. However, these details of the resulted AR and radiated far-field components are always illustrated independently and difficult to evaluate as whole.

In this letter, to evaluate the resulted AR and the far-field components as whole for the radiated planar wave from the antenna, it is found that by showing the radiated far-field components in the AR contour, the resulted AR and the resolved far-field orthogonal components can be simultaneously evaluated. Key information of the far-field orthogonal components, including the phase-advance, phase-lag, power-advance, and power-lag, can be simultaneously observed along with the resulted AR. To utilize this design concept, a broadband CP antenna is designed by directly using the radiated far-field components instead of using the traditional AR curve to achieve broad AR bandwidth. The designed CP antenna was also fabricated and measured for the final performance verification. The design example proves that the method of using the AR contour is very effective and informative for the design of the broadband CP antenna.

II. AR Contour

In this work, the AR contour is first utilized as an effective and informative method to design CP antenna. Suppose that a far-field electromagnetic plane wave radiated from an antenna is propagating toward the +z direction in the Cartesian coordinate system, the plane wave can be resolved into the two orthogonal components, x-axis polarized wave (E_x) and y-axis polarized wave (E_y). The relation between the x-axis polarized wave and y-axis polarized wave here is defined as

$$\frac{E_x}{E_y} = Me^{j\phi} \tag{1}$$

This work was supported in part by China Research Institute of Radiowave Propagation, in part by EPSRC grants EP/N032497/1, EP/P015840/1, and EP/S005625/1, and in part by China Scholarship Council. *(Corresponding author: Lehu Wen.)*

L. Wen, S. Gao, and B. Sanz-Izquierdo are with the School of Engineering and Digital Arts, University of Kent, Canterbury, CT2 7NT, U.K. (e-mail: lw347@kent.ac.uk)

Q. Luo is with the School of Physics, Engineering and Computer Science, University of Hertfordshire, Hatfield, AL10 9AB, UK.

W. Hu is with the National Key Laboratory of Antennas and Microwave Technology, Xidian University, Xian, 710071, China.

where M is the magnitude ratio of these two orthogonal components (E_x and E_y), and ϕ is the corresponding phase difference between E_x and E_y. Therefore, the AR of this plane wave can be expressed as the function of M and ϕ [16], that is

$$AR = \sqrt{\frac{1 + M^2 + \sqrt{1 + M^4 + 2M^2\cos(2\phi)}}{1 + M^2 - \sqrt{1 + M^4 + 2M^2\cos(2\phi)}}} \qquad (2)$$

By using (2), the relation of M and ϕ under the arbitrary constant AR can be obtained, then the contours of different AR values can be plotted in a figure. The resulted different AR contours are shown in Fig. 1. Note that Fig. 1 (a) and Fig. 1 (b) represent the right-hand polarized wave and left-hand polarized wave respectively. For the right-hand polarized wave shown in Fig. 1 (a), the center of the contour stands for the power difference between E_x and E_y is 0 dB, and the corresponding phase difference is the exact 90°. Therefore, an ideal right-hand CP wave is realized in the center of the contour. It can also be observed in the figure that if the phase difference (ϕ) keeps exactly 90°, the power difference (M in dB) equals the resulted AR (in dB). If the power difference is exactly 0 dB, the phase difference of the resulted AR less than a given value will be determined and confined by the according AR contour. Similar characteristics can also be obtained for the left-hand polarized wave shown in Fig. 1 (b).

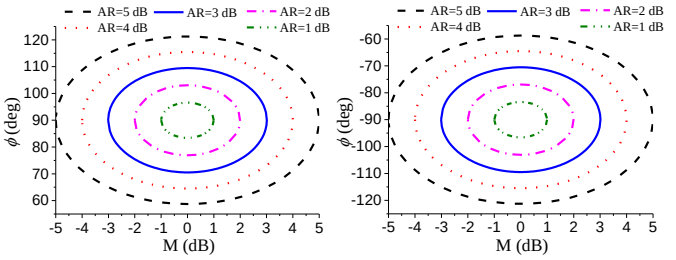

Fig. 1. The relations between M and ϕ when AR equals 5 dB, 4 dB, 3dB, 2 dB, and 1 dB. (a) Right-hand polarized wave. (b) Left-hand polarized wave.

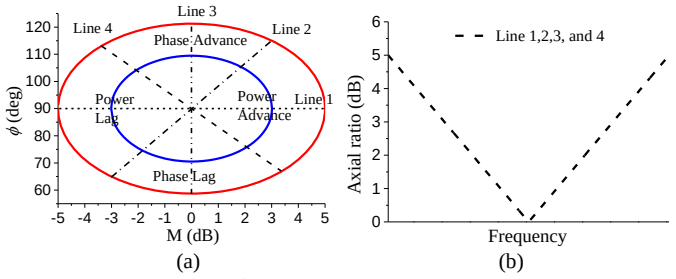

Fig. 2. (a) Background information obtained in the AR contour. (b) The calculated AR versus frequency of four lines in the left figure.

By plotting phase difference versus power difference figure and shown with the AR contour, more background information can be observed compared to the single AR curve. As shown in Fig. 2 (a), four different zones are observed and split by Line 1 and Line 3 in the coordinate system. Line 1 is the constant line of ϕ=90°, which splits the plane into the top phase-advance zone and the bottom phase-lag zone. Line 3 is the constant line of M=0 dB, which splits the plane into the left power-lag zone and the right power-advance zone. In the figure, Line 2 and Line 4 are the arbitrary straight lines passing through the boundary of constant AR=5 dB contour and the center point as the straight Line 1 and Line 3. It can be seen that although straight Lines 1, 2, 3, and 4 have different phase and power changing characteristics as shown in Fig. 2 (a), they have the same AR responses versus frequency, which are shown in Fig. 2 (b). In the traditional design of CP antenna, AR versus frequency curve is commonly used for the direct and intuitive research method as shown in Fig. 2 (b). However, it omits the important information of the phase and power variance characteristics of the radiated far-field components. In this work, these background far-field details are elaborately combined with the resulted AR contour to design CP antenna with increased far-field information and design effectiveness.

III. Antenna Design

In this section, a broadband CP antenna is designed as an example to demonstrate the above design concept to illustrate how to design a CP antenna directly using the radiated far-field components instead of the traditional single AR versus frequency curve.

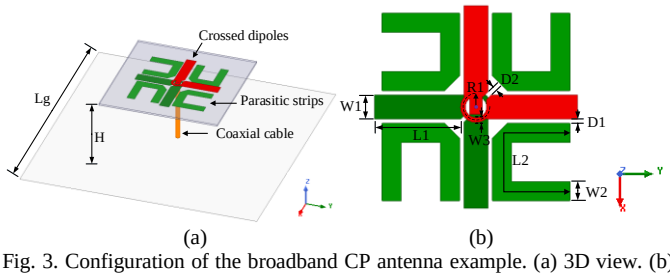

Fig. 3. Configuration of the broadband CP antenna example. (a) 3D view. (b) Top view of the antenna radiator. (Parameters of the antenna configuration. Lg=120 mm, H=30 mm, W1=5 mm, L1= 17.8 mm, W2=4 mm, L2=40 mm, D1=0.9 mm, R1=2.7 mm, W3=1 mm, D2=1 mm.)

Fig. 3 (a) shows the 3D view of a design example of a broadband CP antenna, which is composed of a radiator printed on a substrate, a coaxial cable to feed the radiator, and a square reflector with the length of Lg and distance of H under the radiator for the unidirectional radiation. In Fig. 3 (b), the radiator consists of the crossed dipoles and the arc-shaped strips for required quadrature phase shift. The arc-shaped strip has the width of W3 and radius of R1. Four rotational and symmetrical C-shaped parasitic strips are utilized to improve the operation bandwidth for CP radiation. The C-shaped strips have the width of W2 and the length of L2. Note that the top layer of the substrate is shown in red colour, and the bottom layer is shown in green colour in the figure. A substrate of Rogers 4003C with the relative permittivity of 3.55 and thickness of 0.813 mm is used for the antenna design. Detailed parameters of this antenna are shown in the caption of Fig. 3.

Fig. 4 (a) shows the design steps of the demonstrated antenna. Ant. 1 is the initial linearly polarized dipole antenna without both the phase delay lines and parasitic strips. Ant. 2 is the crossed dipole antenna with only circular phase delay lines. Ant. 3 is the final demonstrated antenna. All these antennas have the same configuration of the reflector. Fig. 4 (b) shows the changing tendency of the far-field components radiated from these antennas. As can be seen, the radiated far-field components of Ant. 1 is dominated by the x-axis polarization with very strong magnitude. To achieve CP radiation, y-axis arranged dipole and phase delay line are incorporated into Ant.

2. So the far-field component curve of Ant .2 moves closely to the small AR=3 dB contour. To improve the AR bandwidth, four C-shaped parasitic strips are introduced and designed near the dipole arms. Therefore, the curve of Ant. 3 is squeezed together forming an AR loop, and is located in the center of AR=3 dB contour with much wider AR bandwidth.

Fig. 4 (c) shows the simulated ARs and S-parameters of these antennas designed step by step. It can be seen that, only one AR minimum is observed for Ant. 2, while two AR minima are obtained for Ant. 3, and the bandwidth is greatly improved. The curves of the reflection coefficient from Ant. 1 to Ant. 3 also show that the impedance bandwidth is gradually improved by using crossed dipoles and C-shaped parasitic strips. The overlapped bandwidth AR<3 dB and $|S_{11}|$<-10 dB is greatly improved from 2.45-2.71 GHz (10% for Ant. 2) to 2.11-2.83 GHz (29% for Ant. 3).

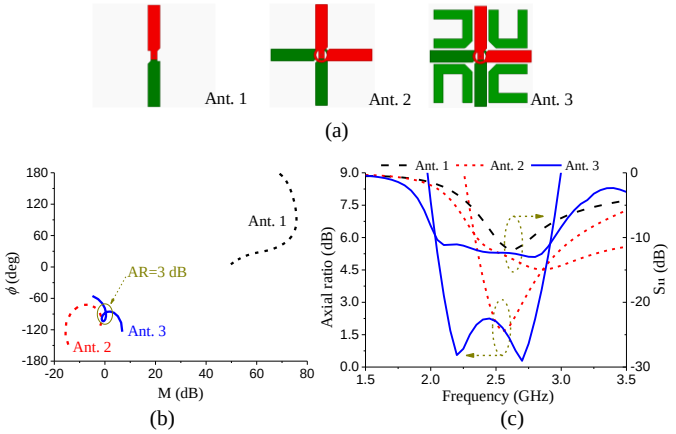

Fig. 4. Design of the demonstrated the antenna step by step. (a) Antennas in each step. (b) Simulated power ratio M and phase difference ϕ. (c) Simulated ARs and S-parameters.

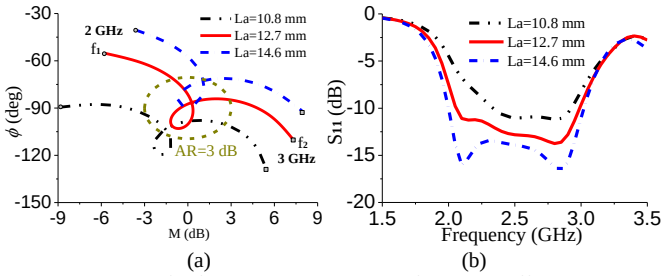

Fig. 5. Simulated far-field components and reflection coefficient vary with different lengths of the phase delay line (Ls). (a) Far-field components. (b) Reflection coefficient.

Along with the AR contour, the AR performance of the CP antenna can be more effectively and informatively designed by using the radiated far-field components as compared to the single AR curve. In this antenna design, different parameters have different effects on the CP performance, and will move the far-field components to different zones or in different directions. To conveniently obtain the optimal AR bandwidth, only AR=3 dB contour is included in the figures for the radiated far-field components. Fig. 5 (a) shows the radiated far-field components vary with the length of the phase delay line (La). Note that La is arc length of the phase delay line (where La=3π×R1/2) in the figure. As shown in the figure, as the increase of the phase delay line, the curve moves obviously along the ϕ-axis with phase-advance. In addition, the curve changes slightly moves along the M-axis. This denotes that the length of the phase delay line not only affects the radiated phase difference of the crossed dipoles, but also slightly affects the magnitude ratio of the radiated x-axis polarized wave to the y-axis polarized wave. Fig. 5 (b) shows the simulated reflection coefficient varies with the length of the phase delay line. The phase delay line can change the input impedance of the antenna. When La is increased from 10.8 mm to 14.6 mm, the reflection at the input port becomes weak and the impedance bandwidth is increased accordingly.

The radiated far-field components and reflection coefficient vary with different lengths of the dipole arm (L1) are shown in Fig. 6. As the increase of L1 shown in Fig. 6 (a), the AR at lower frequency moves towards the AR=3 dB contour, whereas the AR at the upper frequency only slightly changes. Note that the increase of L1 makes the warped AR loop in the AR contour growing bigger, which can be utilized to increase the AR bandwidth. Fig. 6 (b) shows the reflection coefficient varies with the length of the dipole arm. As the increase of L1, the bandwidth at the lower band is increased obviously. However, the reflection coefficient at the upper band is nearly unchanged. This means that the dipole length mainly controls the resonance at the lower band.

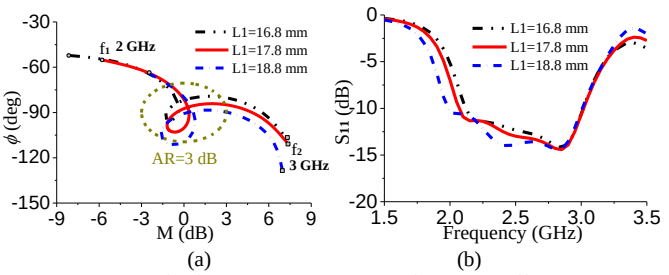

Fig. 6. Simulated far-field components and reflection coefficient vary with different lengths of the dipole arm (L1). (a) Far-field components. (b) Reflection coefficient.

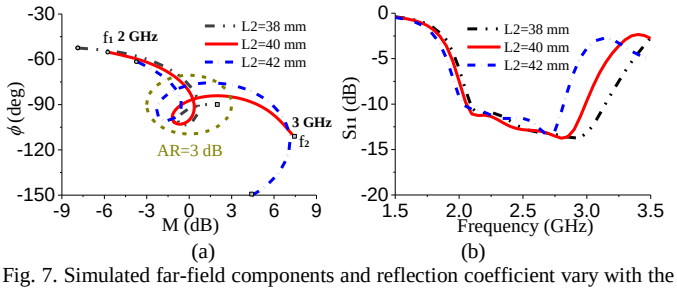

Fig. 7. Simulated far-field components and reflection coefficient vary with the different length of the C-shaped strips (L2). (a) Far-field components. (b) Reflection coefficient.

Fig. 7 shows the effects of the parameters of the parasitic C-shaped strips on the radiated far-field components and S-parameters of the CP antenna. As shown in Fig. 7 (a), when the length of the C-shaped strips (L2) increases from 38 mm to 42 mm, the AR at the lower frequency moves towards the AR=3 dB contour, but the AR at the upper frequency moves away from the AR=3 dB contour. In addition, the AR at the upper frequency changes moves more obviously as compared to the lower frequency. This denotes that L2 has a more significant influence on the AR at the upper frequency. In addition, the warped AR loop in the AR=3 dB contour becomes

bigger as the increase of L2, which can also be utilized to increase the AR bandwidth. Fig. 7 (b) shows the simulated reflection coefficient varies with the parameters of the parasitic C-shaped strips. When the length of the C-shaped strips is increased, the resonance at the upper band shifts to the lower frequency, which causes the impedance bandwidth is decreased. Whereas the resonance at the lower band is slightly changed as compared to the resonance at the upper band.

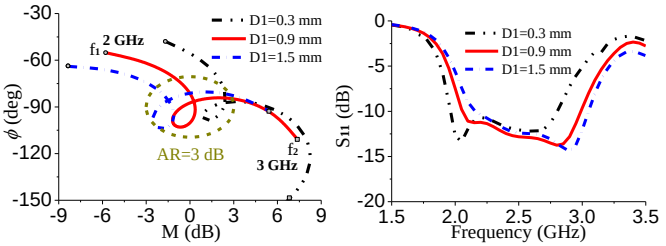

Fig. 8. Simulated far-field components and reflection coefficient vary with the different coupling distances (D1). (a) Far-field components. (b) Reflection coefficient.

The effect of the coupling distance D1 between the parasitic strips and the crossed dipoles on the radiated far-field components of the CP antenna is shown in Fig. 8 (a). The coupling distance has a more direct effect on the magnitude ratio of the x-axis polarized wave to the y-axis polarized wave. As the increase of D1, the AR curve in the AR=3 dB contour moves almost horizontally towards the power-lag zone and along the M-axis. This means that the coupling distance (D1) can be used to adjust the magnitude ratio of two orthogonally radiated waves, but has little effect on the phase difference of the radiated waves. Fig. 8 (b) shows the reflection coefficient varies with the different coupling distances (D1) between the dipole arm and the parasitic strips. As the decrease of D1 (It means the coupling is intensified), the impedance bandwidth shifts to the lower frequency in general. It can be observed that the reflection at the center band is almost unchanged, but improved at the lower band and deteriorated at the upper band. Through the detailed parameter studies shown in Fig. 5 to Fig. 8, it will be easy to develop a broad overlapped impedance and AR bandwidth for the CP antenna.

IV. Measured Results

The broadband CP antenna was fabricated and measured to verify the design concept. Fig. 9 shows the photograph of the fabricated prototype. The S-parameter of the CP antenna was measured by the Anritsu 37397C vector network analyzer, and the AR was measured in the ASYSOL far-field antenna measurement system at University of Kent. Fig. 10 (a) shows the measured and simulated ARs and reflection coefficients of the fabricated prototype. As can be seen, the measured working frequency band slightly shifts to the higher frequency, but the variance tendency agrees well with the simulated results. The measured impedance bandwidth for $|S_{11}|$<-10 dB is from 2.07 GHz to 3.01 GHz. The measured AR bandwidth for AR<3 dB is from 2.15 GHz to 2.93 GHz with two AR valleys.

The measured and simulated far-field components of the power ratio M and phase difference ϕ are also shown in Fig. 10 (b) for a good comparison. The expected warped AR loop is measured and observed within the AR=3 dB contour. As can be seen, the AR curve slightly shifts to the top left part of the figure because of the shift of the working frequency band. However, the AR curve variance tendency agrees reasonably with the simulated AR curve. Fig. 11 shows the measured and simulated radiation patterns in xz plane at 2.2 GHz, 2.5 GHz, and 2.9 GHz. As can be seen, good agreement can be obtained between these results. High radiation efficient is achieved with the measured value higher than 90% within the bandwidth. The slight difference between the measured and simulated results may be caused by the fabrication tolerance and measurement errors in the lab.

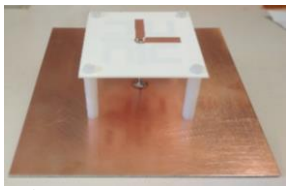

Fig. 9. Photograph of the fabricated prototype.

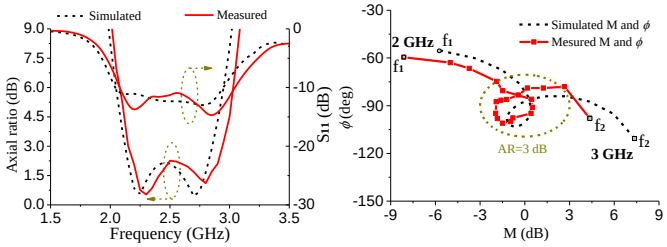

Fig. 10. (a) Measured and simulated ARs and S_{11} of the fabricated prototype. (b) Measured and simulated power ratio M and phase difference ϕ shown in the AR=3 dB contour.

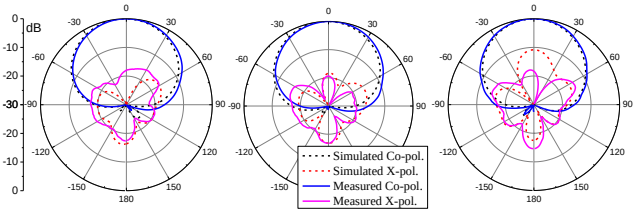

Fig. 11. Measured and simulated radiation patterns at (a) 2.2 GHz, (b) 2.5 GHz, and (c) 2.9 GHz.

V. Conclusion

This paper proposes a method of using AR contour to design a broadband CP antenna. By resolving the radiated CP wave into the two orthogonally polarized waves, the phase difference and power difference of the far-field components will be determined by its related AR contour. A series of AR contours can be obtained for different AR values of the radiated wave. Details of phase-advance, phase-lag, power-advance, and power-lag of the radiated far-field orthogonal components can be observed along with the resulted AR. A broadband CP antenna is then designed and demonstrated by directly using the radiated far-field components instead of the traditional AR versus frequency curve to achieve the broad AR bandwidth for the first time. The design example demonstrates that the method of using the AR contour is very effective and informative to design the broadband CP antenna.

REFERENCES

[1] S. Gao, Q. Luo, and F. Zhu, *Circularly Polarized Antennas*. Hoboken, NJ, USA: Wiley, 2013.

[2] Y. He, W. He, and H. Wong, "A wideband circularly polarized cross-dipole antenna," *IEEE Antennas Wireless Propag. Lett.*, vol. 13, pp. 67-70, 2014.

[3] X. Liang *et al*., "Wideband circularly polarized antenna with dual-mode operation," *IEEE Antennas Wireless Propag. Lett.*, vol. 18, no. 4, pp. 767-770, April 2019.

[4] G. Feng, L. Chen, X. Xue, and X. Shi, "Broadband circularly polarized crossed-dipole antenna with a single asymmetrical cross-loop," *IEEE Antennas Wireless Propag. Lett.*, vol. 16, pp. 3184-3187, 2017.

[5] L. Wang, W. Fang, Y. En, Y. Huang, W. Shao, and B. Yao, "Wideband circularly polarized cross-dipole antenna with parasitic elements," *IEEE Access*, vol. 7, pp. 35097-35102, 2019.

[6] Z. Zhao, Y. Li, M. Xue, L. Wang, Z. Tang, and Y. Yin, "Design of wideband circularly polarized crossed-dipole antenna using parasitic modified patches," *IEEE Access*, vol. 7, pp. 75227-75234, 2019.

[7] A. Dadgarpour, M. Sharifi Sorkherizi, and A. A. Kishk, "High-efficient circularly polarized magnetoelectric dipole antenna for 5G applications using dual-polarized split-ring resonator lens," *IEEE Trans. Antennas Propag.*, vol. 65, no. 8, pp. 4263-4267, Aug. 2017.

[8] Q. Yang, X. Zhang, N. Wang, X. Bai, J. Li, and X. Zhao, "Cavity-backed circularly polarized self-phased four-loop antenna for gain enhancement," *IEEE Trans. Antennas Propag.*, vol. 59, no. 2, pp. 685-688, Feb. 2011.

[9] R. Li, B. Pan, A. N. Traille, J. Papapolymerou, J. Laskar, and M. M. Tentzeris, "Development of a cavity-backed broadband circularly polarized slot/strip loop antenna with a simple feeding structure," *IEEE Trans. Antennas Propag.*, vol. 56, no. 2, pp. 312-318, Feb. 2008.

[10] L. Zhang, S. Gao, Q. Luo, P. R. Young, W. Li, and Q. Li, "Inverted-S antenna with wideband circular polarization and wide axial ratio beamwidth," *IEEE Trans. Antennas Propag.*, vol. 65, no. 4, pp. 1740-1748, April 2017.

[11] Y. Yang, B. Sun and J. Guo, "A low-cost, single-layer, dual circularly polarized antenna for millimeter-wave applications," *IEEE Antennas Wireless Propag. Lett.,* vol. 18, no. 4, pp. 651-655, April 2019.

[12] L. Wen et al., "A wideband series-fed circularly polarized differential antenna by using crossed open slot-pairs," *IEEE Trans. Antennas Propag.,* vol. 68, no. 4, pp. 2565-2574, April 2020.

[13] Z. Zhang, N. Liu, J. Zhao and G. Fu, "Wideband circularly polarized antenna with gain improvement," *IEEE Antennas Wireless Propag. Lett.,* vol. 12, pp. 456-459, 2013.

[14] L. Wen, S. Gao, Q. Luo, W. Hu and Y. Yin, "Wideband dual circularly polarized antenna for intelligent transport systems," *IEEE Trans. Veh. Technol.,* vol. 69, no. 5, pp. 5193-5202, May 2020.

[15] W. Hu et al., "Wideband circularly polarized antenna using single-arm coupled asymmetric dipoles," early accessed in IEEE Trans. Antennas Propag.

[16] C. A. Balanis, *Antenna Theory: Analysis and Design*, 3rd ed. Hoboken, NJ, USA: Wiley, 2005.